A&A 542, A24 (2012)
DOI: 10.1051/0004-6361/201118682

Astronomy & Astrophysics

Pulsation spectrum of δ Scuti stars: the binary HD 50870 as seen with CoRoT and HARPS⋆

L. Mantegazza[1], E. Poretti[1], E. Michel[2], M. Rainer[1], F. Baudin[3], A. García Hernández[4], T. Semaan[5], M. Alvarez[6], P. J. Amado[4], R. Garrido[4], P. Mathias[7], A. Moya[8], J. C. Suárez[4], M. Auvergne[2], A. Baglin[2], C. Catala[2], and R. Samadi[2]

[1] INAF – Osservatorio Astronomico di Brera, Via E. Bianchi 46, 23807 Merate, Italy
e-mail: luciano.mantegazza@brera.inaf.it
[2] LESIA, UMR 8109, Observatoire de Paris, 5 place Jules Janssen, 92195 Meudon Cedex, France
[3] Institut d'Astrophysique Spatiale, CNRS, Université Paris XI UMR 8617, 91405 Orsay, France
[4] Instituto de Astrofísica de Andalucía (CSIC), Glorieta de la Astronomía S/N, 18008 Granada, Spain
[5] GEPI, Observatoire de Paris, CNRS, Université Paris Diderot, 5 place Jules Janssen, 92195 Meudon, France
[6] Observatorio Astronómico Nacional, Instituto de Astronomia, UNAM, Apto Postal 877, Ensenada, BC 22860 México, Mexico
[7] Institut de Recherche en Astrophysique et Planétologie, UMR 5277, 57 avenue d'Azereix, 65000 Tarbes, France
[8] Departamento de Astrofísica, Centro de Astrobiología (INTA-CSIC), PO Box 78, 28691 Villanueva de la Cañada, Madrid, Spain

Received 19 December 2011 / Accepted 15 February 2012

ABSTRACT

Aims. We present the results obtained with the CoRoT satellite for HD 50870, a δ Sct star which was observed for 114.4 d. The aim of these observations was to evaluate the results obtained for HD 50844, the first δ Sct star monitored with CoRoT, on a longer time baseline.
Methods. The 307,570 CoRoT datapoints were analysed with different techniques. The photometric observations were complemented over 15 nights of high-resolution spectroscopy with HARPS on a baseline of 25 d. These spectra were analysed to study the line profile variations and to derive the stellar physical parameters. Some *uvby* photometric observations were also obtained to better characterize the pulsation modes.
Results. HD 50870 proved to be a low-amplitude, long-period spectroscopic binary system seen almost pole-on ($i \simeq 21°$). The brighter component, which also has the higher rotational velocity ($v \sin i$ = 37.5 km s^{-1}), is a δ Sct-type variable with a full light amplitude variation of about 0.04 mag. There is a dominant axisymmetric mode (17.16 d^{-1}). Moreover, there are two groups of frequencies (about 19) in the intervals 6−9 and 13−18 d^{-1}, with amplitudes ranging from a few mmag to 0.3 mmag. After the detection of about 250 terms (corresponding to an amplitude of about 0.045 mmag) a flat plateau appears in the power spectrum in the low-frequency region up to about 35 d^{-1}. We were able to detect this plateau only thanks to the short cadence sampling of the CoRoT measurements (32 s). The density distribution vs. frequency of the detected frequencies seems to rule out the possibility that this plateau is the result of a process with a continuum power spectrum. The spacings of the strongest modes suggest a quasi-periodic pattern. We failed to find a satisfactory seismic model that simultaneously matches the frequency range, the position in the HR diagram, and the quasi-periodic pattern interpreted as a large separation. Nineteen modes were detected spectroscopically from the line profile variations and associated to the photometric ones. Tentative ℓ, m values have been attributed to the modes detected spectroscopically. Prograde as well as retrograde modes are present with ℓ values up to 9. There are no traces of variability induced by solar-like oscillations.

Key words. stars: oscillations – binaries: spectroscopic – stars: interiors – asteroseismology – stars: variables: δ Scuti – stars: individual: HD 50870

1. Introduction

δ Sct stars are multimode low-amplitude, short-period, opacity-driven pulsators in the lower part of the Cepheid instability strip. Recent photometric observations performed by the CoRoT (COnvection, ROtation and planetary Transits) satellite (Baglin et al. 2006) have shown that about 1000 significant peaks have to be removed to obtain amplitude spectra that show noise only (Poretti et al. 2009; García Hernández et al. 2009). In particular, the lowest modes tend to constitute a flat plateau with a high-frequency cut-off (e.g., around 30 d^{-1} for HD 50844) after the simultaneous fit and prewhitening of the strongest ones.

The physical interpretation of this fact leads to two main possibilities. This bunch of peaks could be explained by the excitation of a large number of modes with a high ℓ combined with an insufficient cancellation effect of the flux variations when integrated over the whole stellar disk (HD 50844, Poretti et al. 2009; Daszynska-Daszkiewicz et al. 2006). In this respect, Lignières & Georgeot (2009) showed how rotation enhances the non-cancellation effects, finding that there are three times more visible modes in a star rotating at $\omega = 0.59\,\omega_K$ than in a non-rotating star. Another possibility is that the plateau is generated by the

⋆ The CoRoT space mission was developed and is operated by the French space agency CNES, with participation of ESA's RSSD and Science Programmes, Austria, Belgium, Brazil, Germany, and Spain. This work is based on ground–based observations made with ESO telescopes at La Silla Observatory under the ESO Large Programmes LP 182.D-0356 and LP 185.D-0056 and on data collected at the Observatorio Astronómico Nacional San Pedro Mártir (Mexico).

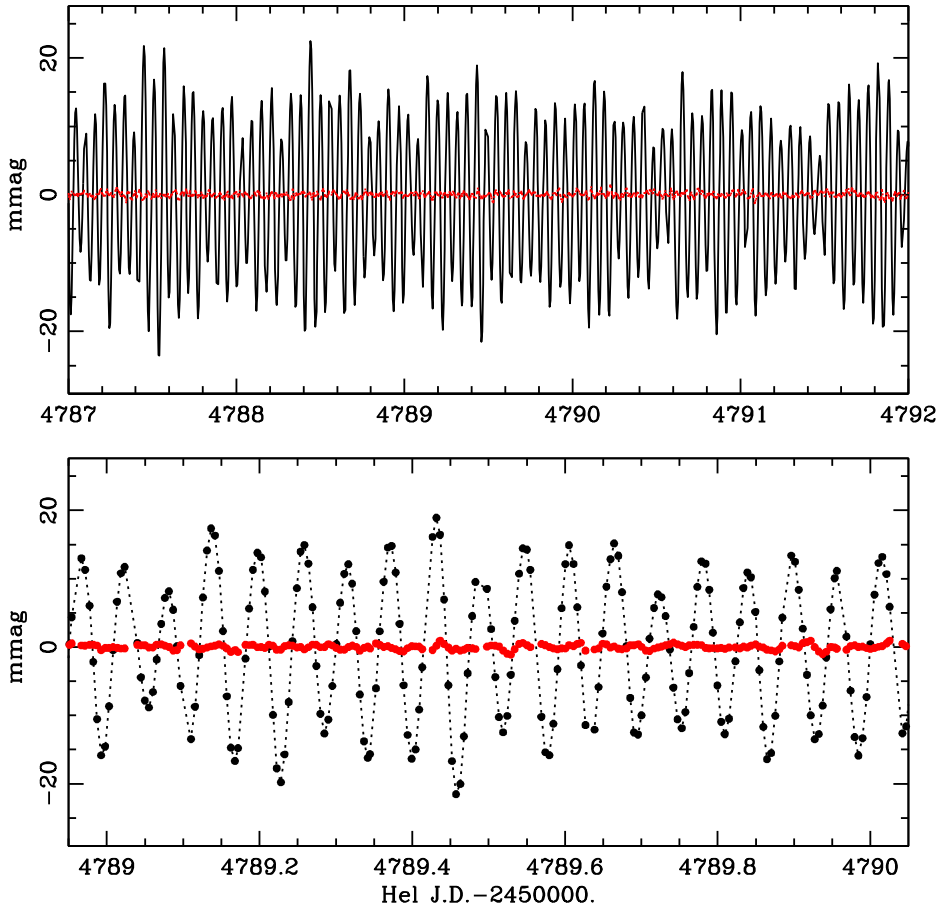

Fig. 1. Examples of the light curve of HD 50870 observed by CoRoT. *The lower panel* is a zoom-in of a region of *the upper panel*. The red points clustering around zero are the residuals after subtracting the 734 detected frequencies.

granulation noise induced by the surface convection (Kallinger & Matthews 2010). In connection with the possible presence of a convective envelope, Antoci et al. (2011) reported the detection of solar-like oscillations in the δ Sct star HD 187547 observed by *Kepler*. Balona & Dziembowski (2011) analysed the *Kepler* data of δ Sct stars and found that in general the frequency density is quite moderate. They suggest that the high density of the frequencies in the HD 50844 data may be an exception.

Additional detailed analyses of the light variation of δ Sct stars are necessary to clarify these open questions. The aim of the present study is add another tile to the assembling mosaic by analysing the CoRoT measurements of HD 50870 ($V = 8.88$, $B - V = +0.27$, F0; McCuskey 1956), a δ Sct discovered in the CoRoT preparatory work (Poretti et al. 2005). To achieve the most complete picture of HD 50870 we complemented the space photometry with ground-based high-resolution spectroscopy and with *uvby* photometry.

2. The CoRoT data and their frequency content

CoRoT monitored HD 50870 in the second long run in the direction of the anticentre (LRa02), started on November 13, 2008 and finished on March 8, 2009 ($\Delta T = 114.41$ d). For the analysis, we used the reduced N2 data rebinned at 32 s and only considered the 307 570 datapoints for which no problem (i.e., flag = 0) was reported. The amplitudes of the background orbital variations were kept at a very small level by the great effectiveness of the baffle, and the subsequent rejection of the uncertain points strongly minimized the orbital effects. The light curve was detrended with a low-degree polynomial fit to remove the effect of ageing (Auvergne et al. 2009).

The original data binning of 32 s is higher than necessary for the relevant frequency range of δ Scuti stars and therefore we grouped the original data into new bins with a time separation of 0.005 d to gain CPU time, thus obtaining 20 535 datapoints and a Nyquist frequency of 100 d^{-1}. An example of the resulting light curve is shown in Fig. 1.

The spectral window is shown in Fig. 2. The positions of the alias peaks is very similar to those in the window of HD 50844; their nature has been carefully discussed by Poretti et al. (2009). Note also how the amplitude spectrum reflects the spectral window above 40 d^{-1}, because of the predominant term at 17.16 d^{-1}.

The detection of the frequencies contributing to the light variations was performed iteratively by computing the Fourier power spectrum (Deeming 1975), selecting the highest peak, adjusting its frequency by a non-linear least-squares fit of all previously detected sinusoidal terms plus the new one, computing the residuals produced by this fit with respect to the original time series and proceeding to the detection of a new term. At each step the amplitude signal-to-noise ratio (S/N) was computed for the new detected term with respect to the average noise in a frequency range of 5 d^{-1} centred around its frequency. The iterations were stopped when a local S/N of 3.0 was reached. This approach is similar to that performed by the Period04 code (Lenz & Breger 2005), but it is made by means of a completely

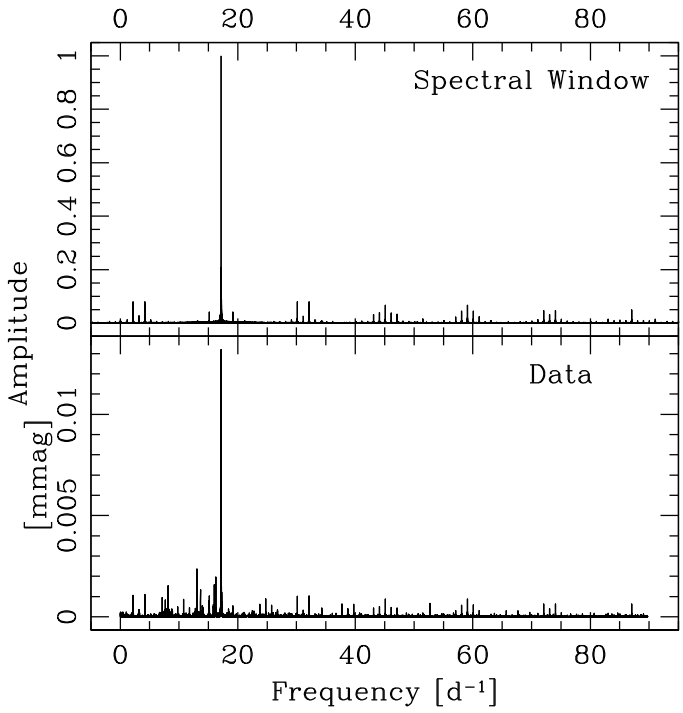

Fig. 2. *Top panel*: the spectral window of the CoRoT data of HD 50870. *Bottom panel*: the amplitude spectrum of the original CoRoT data after the removal of the slow trend.

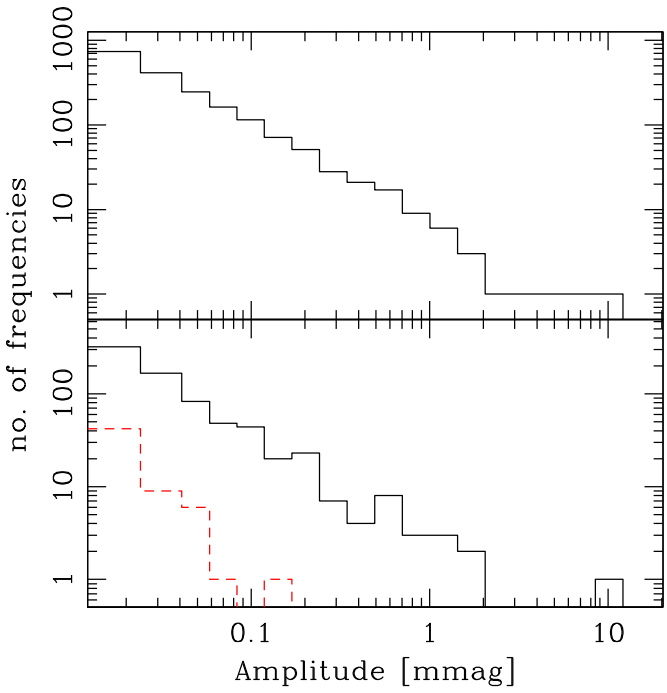

Fig. 3. Distribution of the frequencies vs. amplitudes. *Top panel*: Number of frequencies with an amplitude higher than a given value. *Bottom panel*: histogram of the 734 frequencies (black solid line); distribution of the frequencies that were not detected by SigSpec (red dashed line). Note the logarithmic scales.

automated f77 code, which also allows detecting more frequencies (Period04 is limited to about 200 components). The frequency analysis was performed using the relative fluxes, then the results were scaled into mmag units.

We detected 734 frequencies with amplitudes ranging from 12.961 mmag down to 0.020 mmag. The distribution of the detected frequencies vs. their amplitudes is shown in Fig. 3. The developments of the analysis are plotted in Fig. 4, where we can see step by step the amplitudes of the detected terms, their local S/N at the detection, and the decrease of the residual rms. These plots allow us to see how many components are needed to go below a certain level of S/N or rms residual or amplitude.

Figure 5 shows how the amplitude spectrum changes its shape at the various stages of the analysis. At first one strong dominant peak is visible at $f_1 = 17.1617$ d^{-1}, then two groups of peaks show up in the ranges 7–9 d^{-1} and 12–18 d^{-1}. Successively, bunches of peaks appear between 0 and 35 d^{-1}. It is only after the detecting of about 250 terms that the 0–35 d^{-1} region becomes a flat plateau, progressively decreasing in height after performing new peak detections. The dominant peak at about 34 d^{-1} in the third panel from the top is the $2f_1$ harmonic, while the isolated peak at about 51 d^{-1} in the fourth and fifth panels from the top is the $3f_1$ harmonic. No higher-order harmonic of f_1 was detected. The white noise level is 0.0031 mmag as estimated in the region 60–90 d^{-1}, which leads to S/N = 6.7 for the plateau below ∼35 d^{-1} visible in the bottom panel of Fig. 5.

The components with an amplitude higher than 0.3 mmag (24 frequencies) are listed in Table 1. Among the detected peaks f_{16} (13.9725 d^{-1}) corresponds to the satellite orbital frequency, while f_{418} (2.0029 d^{-1}, 0.037 mmag) could be produced by the gaps introduced in the timeseries by the transit of the satellite through the South Atlantic Anomaly (SAA), and therefore they are probably not attributable to the star. In the solution of HD 50870 we find some frequencies with a high rank of detection that exactly match the linear combination between a

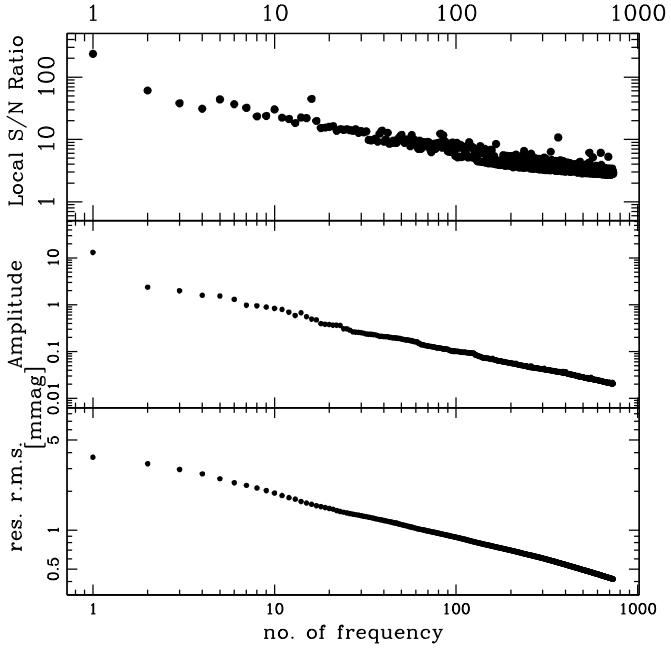

Fig. 4. Evolution of the frequency analysis of the CoRoT time series. *Top panel*: local S/N of the *n*th highest peak. *Middle panel:* amplitude of the *n*th highest peak. *Bottom panel*: residual rms after subtracting all detected frequencies up to *n*th term. Note the logarithmic scales on both axes. In the top panel the two points with the largest deviations are the Fourier harmonics of the dominant mode.

lower-rank frequency and the first, predominant term f_1 (last column in Table 1). They probably arise from nonlinear amplitude distortion and are commonly found in multiperiodic radial pulsators (Cepheids, RR Lyr, high-amplitude δ Sct stars) as well as in low-amplitude δ Sct stars, e.g. FG Vir (Breger et al. 2005).

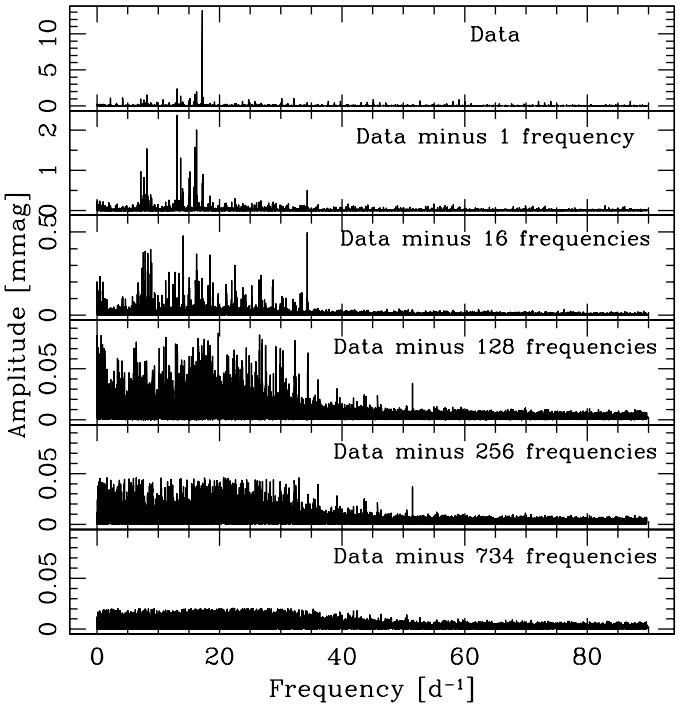

Fig. 5. Fourier amplitude spectra at different stages of the analysis. The flat plateau below about 35 d^{-1} appears after the detection of about 250 frequencies. The highest peak in the third panel from top is the second harmonic of the dominant frequency, while its third harmonic is the peak at the highest frequency in 4th and 5th panel.

Table 1. First 24 frequencies identified in the amplitude spectrum (those with an amplitude >0.3 mmag).

Term	Frequency [d^{-1}]	Frequency [μHz]	Ampl. [mmag]	Possible combination terms
f_1	17.1617	198.630	12.961	$f_{16} = 2f_1$, $f_{365} = 3f_1$
f_2	13.0499	151.040	2.342	$f_{87} = f_1 + f_2$, $f_{104} = f_1 - f_2$ $f_{726} = 2f_2$
f_3	16.2507	188.086	1.736	$f_{82} = f_1 + f_3$
f_4	16.0024	185.212	1.593	$f_{85} = f_1 + f_4$, $f_{150} = f_1 - f_4$
f_5	8.1366	94.173	1.544	$f_{96} = f_1 + f_5$, $f_{447} = 2f_5$, $f_{597} = 3f_5$
f_6	13.6605	158.107	1.313	$f_{95} = f_1 + f_6$, $f_{190} = f_1 - f_6$
f_7	7.1320	82.546	0.974	$f_{356} = f_1 + f_7$, $f_{554} = 2f_7$, $f_{721} = 3f_7$
f_8	15.1787	175.678	0.979	$f_{136} = f_1 + f_8$
f_9	17.2805	200.005	0.903	$f_{167} = f_1 + f_9$, $f_{187} = f_9 - f_1$
f_{10}	7.6604	88.661	0.824	$f_{115} = 2f_{10}$, $f_{178} = f_1 + f_{10}$
f_{11}	15.0390	174.061	0.836	
f_{12}	16.2473	188.046	0.819	
f_{13}	17.1863	198.914	0.692	
f_{14}	15.8344	183.267	0.726	
f_{15}	15.8217	183.120	0.707	
f_{16}	13.9725	161.718	0.792	
f_{17}	34.3232	397.257	0.501	
f_{18}	14.0608	162.740	0.471	
f_{19}	8.7541	101.320	0.390	
f_{20}	7.8843	91.253	0.384	$f_{269} = 2f_{20}$, $f_{284} = 3f_{20}$
f_{21}	18.4425	213.453	0.377	
f_{22}	8.2945	96.001	0.371	
f_{23}	7.5452	87.328	0.324	$f_{60} = 2f_{23}$
f_{24}	8.8886	102.877	0.308	$f_{70} = 2f_{24}$, $f_{505} = 3f_{24}$

Notes. The last colum indicates possible combination terms also present in the data.

The sums and, in some cases, the differences are detected for the modes up to f_{10}. The identification of some high-rank frequencies with the harmonics of low-amplitude terms (f_{20}, f_{23}, and f_{24}) is reported in Table 1 as a mere possibility, since they are embedded in the flat plateau below 35 d^{-1} and an accidental agreement could occur.

The data were also analysed with the SigSpec code (Reegen 2007). To go below S/N = 4.0 (corresponding to a value of the *sig* parameter of about 5.46), SigSpec requires 790 frequencies. The difference in the number of significant peaks with respect to the Fourier analysis is probably due to the different approaches in computing the white noise level. When comparing the two approaches, we found that 673 of the 734 frequencies detected with the Fourier analysis are at a distance shorter than 0.0044 d^{-1} (half the formal frequency resolution) from the corresponding frequency detected with SigSpec. In turn, this means that 61 frequencies detected with Fourier were not detected with SigSpec. The first missed detection is the 141-th frequency, whose amplitude is 0.090 mmag. The histogram with the detections missed by SigSpec vs. the Fourier amplitudes is shown in Fig. 3. Since the 734 detected frequencies are concentrated in the interval 0−35 d^{-1}, the probability of randomly finding two independent frequencies in the same resolution bin with the two approaches is less than 0.2.

To check the reliability of the detected frequency terms with the highest amplitude, the dataset was subdivided into two equal subsets, each with a length of half the original baseline. Each subset was analysed independently and the detected frequencies were compared with those obtained from the whole dataset. Of the first 150 frequencies detected from the whole dataset 146 were independently detected from the two subsets. The missing components are the number 100, 129, 133, and 137. Component number 100 has a frequency of 13.0601 d^{-1}, and is therefore not resolved in the subsets from the second (13.0499 d^{-1}). The other three missing frequencies were in any case independently detected in one of the two subsets.

The very recent result by Antoci et al. (2011) concerning the detection of solar–like oscillations in the δ Sct star HD 187547 prompted us to look carefully at the power spectra of HD 50870. HD 187547 shows solar-like frequencies in the range of 43−73 d^{-1} (i.e., 500−850 μHz) with amplitudes up to 0.15 mmag, while the δ Sct oscillations are confined to frequencies lower than about 48 d^{-1} (550 μHz). The physical parameters of the two stars, as estimated from their spectra and multicolour photometry, are quite similar, which is also supported by the frequency ranges covered by the highest-amplitude modes in both stars. We should therefore expect to find solar–like frequencies in the same region. For HD 50870 all detected frequencies are confined below 51.5 d^{-1} (~600 μHz). No significant peak is present above this limit. We estimated the white noise level there to be at about 3 ppm. Only five of the detected frequencies above 35 d^{-1} have amplitudes higher than 20 μmag. One of them is the third harmonic of the predominant mode and the others are still close to the limit of 35 d^{-1}. Moreover, a frequency analysis performed on the data with the original binning of 32 s showed that in the frequency region between 90 and 500 d^{-1} there are no peaks with an amplitude higher than 6 μmag. Since there is no regular spacing, the frequency analysis of the CoRoT data on HD 50870 does not supply any hint of the excitation of solar–like oscillations at first sight.

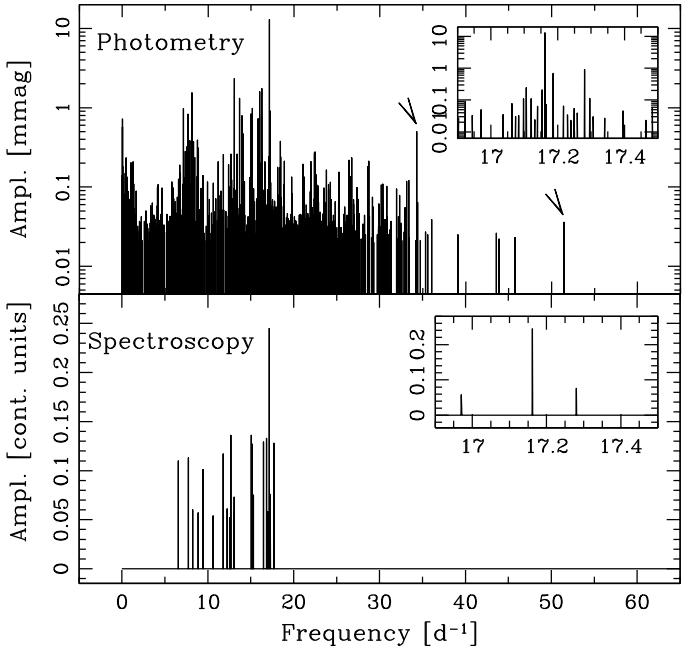

Fig. 6. Distribution of the 734 frequencies detected in the CoRoT data (*top panel*) and of the 19 detected in spectroscopy below the pseudo-Nyquist frequency of 21.06 d^{-1} (*bottom panel*). In the top panel the two arrows show the second and third harmonics of the predominant mode. The insets show a zoom around the predominant frequency.

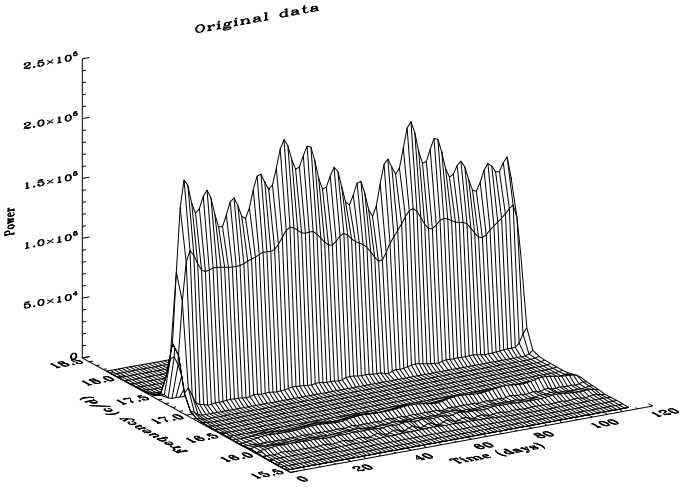

Fig. 7. Amplitude behaviour vs. time of the oscillations in the frequency range [15.5,18.5] d^{-1} (i.e., around the dominant mode).

2.1. Amplitude stability

It is rewarding to investigate the stability of the amplitude of the predominant mode f_1 = 17.17 d^{-1}. To do this, we need to consider that the modes f_9 = 17.28 d^{-1} and f_{13}=17.19 d^{-1} are close to f_1. Figure 7 shows the variation of amplitude recorded when the amplitude modulation is calculated with a frequency resolution of 0.17 d^{-1}, which is insufficient to resolve the three components.

The modulation of the amplitude is clear, but spurious, because it results from the beating of the unresolved components. We built a synthetic time series using the constant values of amplitudes, frequencies, and phases given in Table 1 for the three components and sampled it in the same way as the CoRoT data. The time-frequency analysis of this synthetic signal shows the same behaviour of the amplitude (Fig. 8), supporting the conclusion that the amplitudes of the f_1, f_9, and f_{13} modes remain constant over the entire time interval covered by the CoRoT observations.

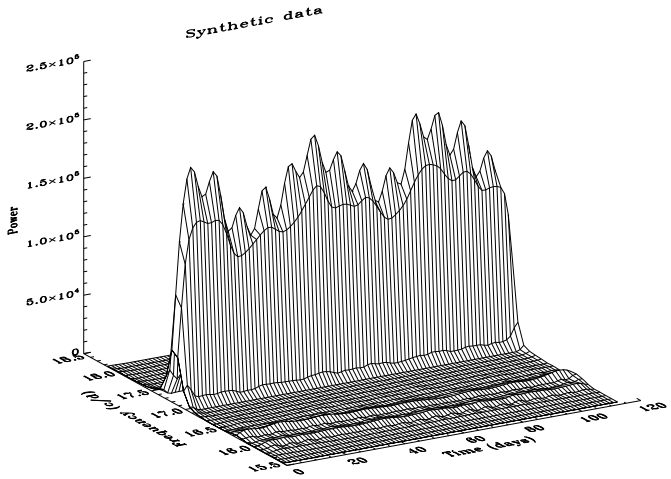

Fig. 8. Amplitude behaviour vs. time of a synthetic signal built with the frequency terms detected in the region of the dominant mode keeping a constant amplitude: there is an excellent agreement with the behaviour derived from the observations.

Modes with a lower amplitude were also analysed searching for the typical random variations of amplitude and phase of stochastically excited (solar-like) oscillations, but none showed this behaviour.

3. Ground-based observations

3.1. High-resolution spectroscopy

The main batch of spectroscopic observations was performed during 15 nights between December 15, 2008 and January 8, 2009 with the HARPS instrument mounted on the 3.6-m ESO telescope, La Silla, Chile. The spectrograph was used in the high-efficiency EGGS mode, with resolution $R \sim 80\,000$. We obtained 209 spectra in two runs (ten and five nights, respectively), covering a baseline of 24.3 d, i.e., 4.7 times shorter than that of CoRoT. The exposure time was set to 1200 s and the S/Ns ranged from 87 to 175 with a median value of 145. The spectra were reduced using a semi-automatic pipeline, written in MIDAS and developed by Rainer (2003). To study the spectral variations induced by pulsation with the highest S/N possible, we computed the mean line profiles using the least-squares deconvolution (LSD) method (Donati et al. 1997) in the spectral region between 4140 and 5615 Å, taking care to omit the intervals containing the H_β and H_γ lines. The resulting LSD profiles have S/Ns ranging from 1260 to 3900 with a mean value of 2406, i.e., the original S/N was increased by a factor of about 17. In Fig. 9 we show the average LSD profile (top panel, black solid line) and the standard deviation of the original LSD profiles (bottom panel, black solid line).

3.2. Evidence for binarity

The average profile shows the superimposition of two components, one narrow and another broader. The close scrutiny of the narrow absorption peak did not show any appreciable movement with respect to the broader component during the baseline

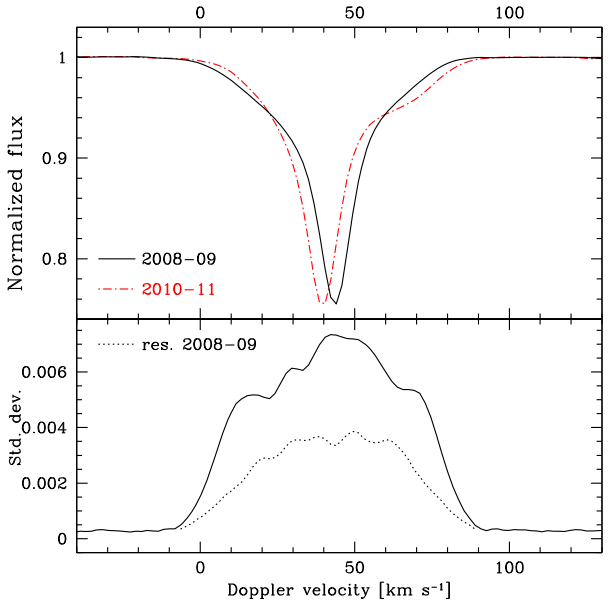

Fig. 9. *Top panel*: average LSD mean profiles of the 2008-09 (black solid line) and of the 2010-11 spectra (red dash-dotted line). *Bottom panel*: standard deviations of the original (solid line) and of the residual (dotted line) 2008-09 LSD profiles.

of 25 d. A non-linear least-squares fit of two Gaussian components was performed on the average profile: the centre of the narrow component is shifted by about 2.7 km s^{-1} towards the red edge of the spectrum with respect to the centre of the broad one.

To clarify the possible binary nature of this object nine new HARPS spectrograms were taken between December 25, 2010 and January 8, 2011 and three more between December 18, 2011 and January 12, 2012. The LSD profiles were obtained as described above and their average shows that while there is no significant difference between the 2010-11 and 2011-12 spectra, the two components have moved compared to the positions in 2008-09 (Fig. 9, top panel). The narrow component is shifted by 5.2 km s^{-1} towards the blue edge in the most recent spectra. There is also a single FEROS spectrogram (R = 48 000) taken with the FEROS spectrograph attached to the 2.2 m-ESO/MPI telescope on January 18, 2003: its LSD profile shows that the narrow component is shifted by 0.9 km s^{-1} towards the red edge. We can conclude that we observe a spectroscopic binary.

We disentangled the spectra with the CRES code (Ilijic 2004) to obtain a reasonably accurate estimate of the physical parameters of the two components. To do this we selected some spectral regions that contained lines that are sensitive to the temperature only or/and to the gravity only in the FEROS spectrogram and in the two average HARPS spectrograms. These spectra were then normalized with the approach described by Ilijic et al. (2004). As an example, Fig. 10 shows the 2008-09 average spectrum in the wavelength range 4487–4492 Å and the two extracted components.

Subsequently, the physical parameters of the two stars were estimated with the SME code (Valenti & Piskunov 1996), which fits the observed spectrum with a synthetic one derived from an interpolation of a grid of models. Estimates of the effective temperatures, gravities, metallicities, microturbolent velocities, and projected rotational velocities were obtained by averaging the result of the different spectral regions (Table 2). Finally, we used the ATC code (Stuetz et al. 2006) to compute two synthetic spectrograms with these parameters and combined them with the BinMag IDL visualization tool (constructed by O. Kochukov) and compared the combined spectrum with the observed average spectrograms (Fig. 11). The Vienna Atomic Line Database VALD (Kupka et al. 2000; Piskunov et al. 1995) was used throughout. The ratio between the luminosities of the two components at 4500 Å is 2.0±0.4. These results should be considered as preliminary only: additional observations that cover more of the orbital period will be able supply firmer results.

3.3. Line profile variations

The detection of pulsation modes in the line profile variations (LPVs) was performed both with the FAMIAS code (Zima 2008) and with the least-squares technique described by Mantegazza (2000) using the pixel-by-pixel approach. No LPVs were detected in the component with the narrow lines. On the other hand, clear LPVs were detected in the component with the broad lines. Figure 12 shows the least-squares power spectrum obtained from the LSD profiles (top panel) and the spectral window of the spectroscopic data. We clearly note that the shorter baseline of the spectroscopic observations (24 d) implies a frequency resolution worse than that of the CoRoT photometric data. Moreover, there are aliases at ±1 d^{-1} from the true peak due to the single-site observations, and because the observations were performed in two separated runs, each spectral peak is flanked by two symmetrical peaks at ±0.051 d^{-1} (Fig. 12, inserted panel in the top panel). This hampers a comparison of the photometric frequencies with the spectroscopic ones, since in some cases there are several photometric frequencies that might be associated to a single spectroscopic peak. This clearly entails more uncertainty on the correct identification of the modes. Moreover, because of the spacing between adjacent spectra, the pseudo-Nyquist frequency is 21.06 d^{-1}. This explains the bunch of peaks around 42 d^{-1} in the spectral window (Fig. 12, top panel) and the peaks around 25 d^{-1} and above 48 d^{-1} in the first power spectrum (middle panel). Because of this, attention was paid to avoid misidentifications of reflected frequency peaks both above and below this value. The comparison of the findings with the two approaches allowed us to identify with some confidence 19 oscillation frequencies (Table 3). All frequencies were associated to a photometric term (first column). There are some ambiguities owing to the different frequency resolution of the photometric and spectroscopic data. Where that was the spectroscopic term was associated to the strongest photometric one that is within the HWHM of the centre of the spectroscopic peak.

The second and third panels of Fig. 12 show the pixel-by-pixel least–squares power spectra of LPVs before and after the frequency detection of the 19 above quoted terms. Figure 9 (bottom panel, dashed red line) shows the standard deviations across the LSD line profile of the residuals obtained by subtracting all the detected components. Evidently, many undetected components are still present.

The amplitude and phase variations of all spectroscopic modes run across the whole line profile (from −10 to 90 km s^{-1}, some examples are shown in Fig. 13): this gives us the certainty that the pulsational variability has to be ascribed to the fast rotator.

The spectroscopic modes are shown in the bottom panel of Fig. 6. The pseudo-Nyquist frequency (21.06 d^{-1}) must be taken into account when comparing them with the photometric counterparts (top panel). The amplitudes (the third column of Table 3) are integrated on the whole LSD profile, while their S/Ns (fourth column) are computed by FAMIAS. The shape of

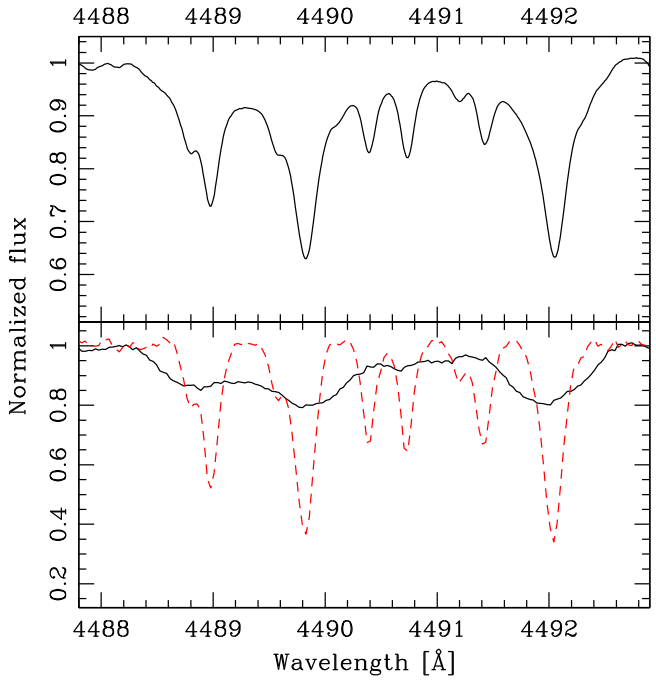

Fig. 10. Example of a small region of the observed spectrum of HD 50870 (*top panel*) and its separation by the CRES code in the spectra of the two components (*bottom panel*).

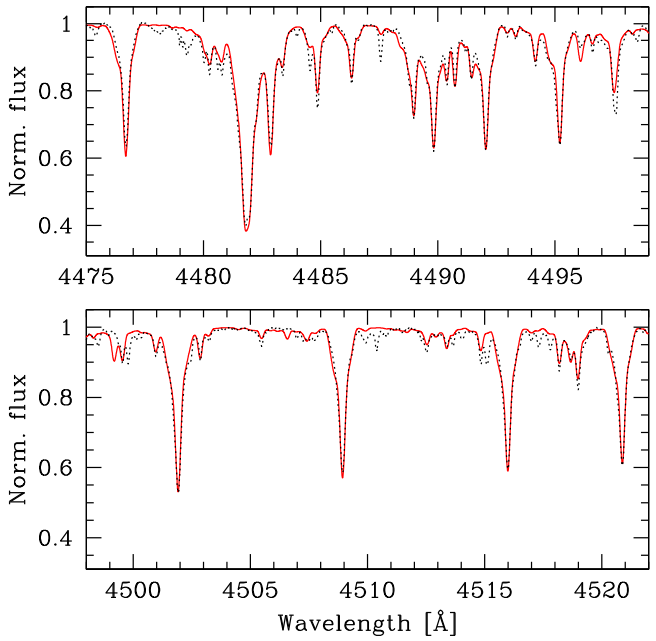

Fig. 11. Example of a comparison between the observed spectrum (black dashed line) and the combination of the synthetic spectra of the two components obtained with the binmag2 code (red solid line).

amplitude and phase curves of the dominant mode (17.1617 d^{-1}, top panel of Fig. 13) looks quite entangled across the line profile, but it seems to be an axisymmetric mode. This probably indicates the presence of another unresolved mode superimposed on the axisymmetric one. Any attempts to fit this peak taking into account other nearby peaks (considering adjacent photometric detections) did not supply significant improvements because of the complexity of the spectral region around f_1 (see Fig. 6).

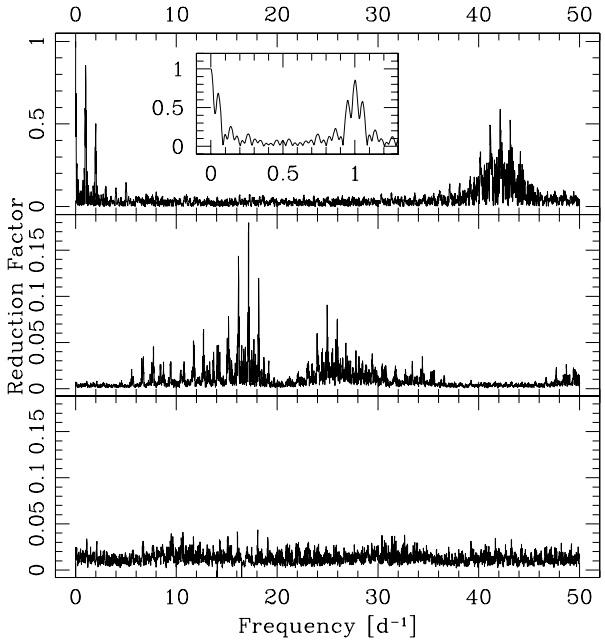

Fig. 12. *Top panel*: spectral window of spectroscopic time-series. The high-resolution view of the fine structure of the peaks is shown in the insert. *Middle panel*: least-squares power spectrum of LPVs of the original data. The ordinatae show the percentual data variance reduction. *Lower panel*: least-squares power spectrum with the 19 detected frequencies given as known constituents. The ordinates show the percentual reduction of the residual data variance after the fit with the known frequencies.

Table 2. Physical parameters of the two components.

	Star 1	Star 2	Uncertainty
$T_{\rm eff}$ [K]	7660	7077	±250
Spectral type	A8 III	F2 III	
log g	3.68	3.74	±0.25
[Fe/H]	0.0	0.0	±0.2
$v_{\rm mic}$ [km s^{-1}]	3.3	2.8	±1.0
$v \sin i$ [km s^{-1}]	37.5	8.0	±2.5

3.4. Line profile moments

An independent search for frequencies was performed on the timeseries defined by the 0th (equivalent width, EW), 1st (radial velocity), and 2nd (line width) order moments. For these computations the narrow absorption profile (approximated by a Gaussian) was subtracted, because the amplitudes of the moment variations are dependent on the average profile shape. Because the moments are integrated over the whole stellar disc, they are more sensitive to low-degree modes. The results are shown in Table 4. We see that the first 15 photometric terms were independently detected at least in one of the moment curves. In particular, all were detected in the radial velocity variations.

All modes detected in the zero-order moments were also detected in the first-order moment and in general correspond to the strongest photometric terms. The only exception is the 8.8886 d^{-1} mode, which probably suffers from the contamination of the 7.8843 d^{-1} mode. That several of the detected modes in the first-order moment were not detected in the second-order one, and in particular among those with the strongest photometric amplitudes, suggests that these could be axisymmetric modes ($m = 0$). The detection of axisymmetric modes is favoured for

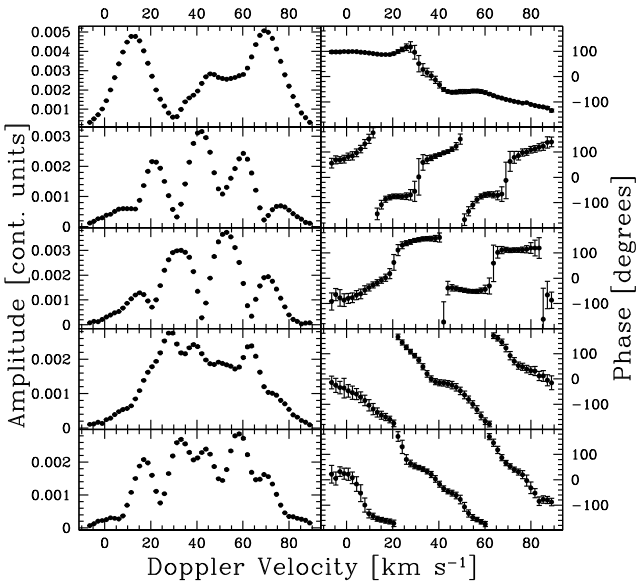

Fig. 13. From *top to bottom*: amplitude (*left panel*) and phase (*right panel*) variations across the line profile of one axisymmetric (17.1617 d^{-1}), two retrograde (7.7262 and 12.6917 d^{-1}), and two prograde modes (16.848 and 16.874 d^{-1}).

Table 3. Mode detected by the line profile variations listed in order of detection.

Term	Frequency [d^{-1}]	Frequency [μHz]	Spectr. Ampl.	S/N	ℓ, m	Phot. Ampl. [mmag]
f_1	17.1616	198.628	0.245	14.8	1,0; 0,0	12.961
f_{11}	15.0390	174.061	0.136	6.5	4,1	0.354
f_{27}	12.6917	146.894	0.136	9.7	6,–2	0.259
f_{196}	16.8485	195.005	0.133	7.3	6,5	0.059
f_{203}	16.4743	190.674	0.129	6.8	7,5	0.064
f_{58}	7.7266	89.428	0.113	8.5	7,–3	0.167
f_{219}	17.6884	204.726	0.128	7.9	6,4	0.051
f_{28}	11.7787	136.327	0.117	8.0	6,–5	0.257
f_{79}	6.5680	76.018	0.110	5.2	5,–2	0.125
f_8	15.1787	175.678	0.127	9.0	4,1	0.979
f_{71}	9.4454	109.321	0.101	5.9	7,–5	0.125
f_9	17.2805	200.005	0.076	5.9	3,1	0.903
f_{115}	15.3171	177.280	0.075	6.5	6,0	0.095
f_{29}	8.2442	95.418	0.060	5.2	9,–5	0.262
f_{24}	8.8886	102.877	0.057	3.0	8,–1	0.308
f_2	13.0499	151.040	0.073	5.0	2,0 (1,0)	2.342
f_{83}	10.6011	122.697	0.054	3.4	7,–3	0.112
f_{218}	16.9705	196.417	0.058	4.7	8,7	0.046
f_{110}	12.5337	145.065	0.052	3.6	7,1	0.094

Notes. All of them were associated to a photometric term.

geometrical reasons because the star is seen almost pole-on (see paragraph 3.5). We point out $f_2 = 13.0499$, $f_3 = 16.2507$, $f_4 = 16.0024$, $f_5 = 8.1366$, and $f_6 = 13.6605$ d^{-1} as the most promising candidates.

The dominant photometric mode (17.1617 d^{-1}) was detected in all moment curves. The variation of the first three moments phased according to the dominant period are compared with the light variations in Fig. 14. However, while f_1 is the strongest term in the zeroth- and first-order moment, it is not the dominant term in the second-order one, where the dominant mode is $f_8 = 15.1787$ d^{-1}. We cannot exclude that there may be

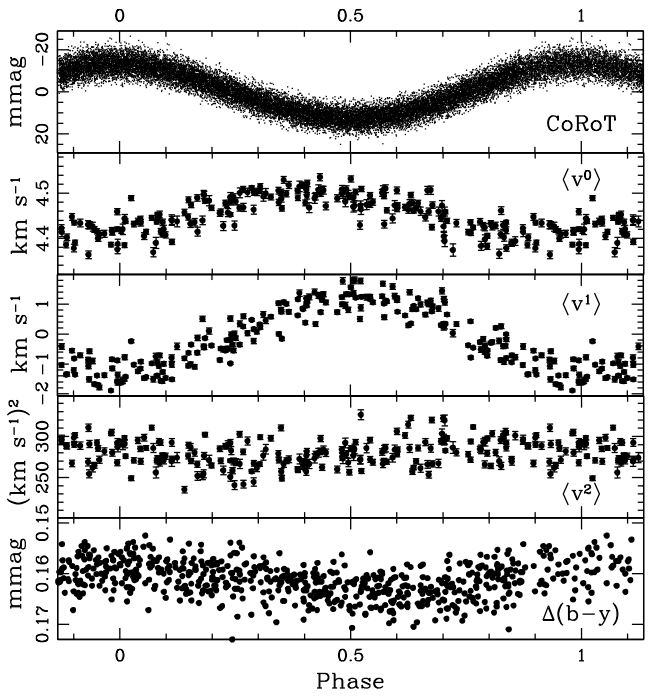

Fig. 14. From *top to bottom*: light, first three moments and $\Delta(b-y)$ (comparison minus variable) variations folded in phase according to the main pulsation frequency $f_1 = 17.1617$ d^{-1}.

a reciprocal partial contamination caused by aliasing, considering that the distance between the two peaks is 1.983 d^{-1}. Maybe this contamination could also explain the perturbed shapes of amplitude and phase variations across the line profile (Fig. 13, top panels).

3.5. Mode identification

It is difficult to accurately fix the stellar physical parameters, considering all the uncertainties connected to the disentanglement of the spectra and the fact that the stellar parallax is unknown. However, if we consider the parameters given in Table 2 to be sufficiently reliable, we can derive from the tables by Straizys & Kuriliene (1981) that the primary star (i.e. the δ Sct variable) has an A8 III spectral classification and therefore a bolometric magnitude of 1.1 ± 0.3 mag. Such a star would lie practically in the centre of the δ Sct instability strip (Breger 2000). With Eq. (6) in Breger (2000) and using $\log g$ and $T_{\rm eff}$ from Table 2 and the above quoted $M_{\rm bol}$, we can estimate that the frequency of the radial fundamental mode ($Q = 0.033$ d) should be about 7.4 ± 2.2 d^{-1}.

From the paper by Schaller et al. (1992) we find, using the above derived $T_{\rm eff}$ and $M_{\rm bol}$ values, a mass of 2.1 ± 0.3 $M_\odot$. Combining this with the estimated $\log g \sim 3.7$, we derive a radius of 3.4 ± 1.2 $R_\odot$, and we adopted this value for the subsequent mode identification. An attempt to derive a more accurate value by applying the Baade-Wesselink technique using light, colour ($b-y$ variations are shown at the bottom of Fig. 14; see Sect. 3.6 for details) and radial velocity variations of the dominant mode (17.17 d^{-1}) did not lead to a significant result. In turn, this supports the $\ell = 1$ identification for the f_1 mode. Only for this ℓ value the projected area variation is null and the Baade-Wesselink technique breaks down (Stamford & Watson 1981).

The mode identification was performed with FAMIAS in the AP mode (see Zima 2008). Since the profiles shapes are

Table 4. Modes detected by the line moment variations.

Term	Frequency		*EW*		Rad. vel.		Line width		Phot. Amp.
	[d^{-1}]	[μHz]	[10^{-2} km s^{-1}]	S/N	[km s^{-1}]	S/N	[km s^{-1}]^2	S/N	[mmag]
f_{79}	6.5680	76.018					4.4	5.8	0.125
f_7	7.1320	82.546			0.08	6.3			0.974
f_{26}	7.3304	84.842			0.06	4.4	3.7	4.8	0.280
f_{10}	7.6604	88.661			0.04	3.0			0.824
f_5	8.1366	94.173	0.66	4.5	0.12	9.4			1.544
f_{24}	8.8886	102.877	0.47	3.5	0.05	3.4	3.7	5.8	0.308
f_2	13.0499	151.040	1.15	11.4	0.24	17.0			2.342
f_{30}	13.3778	154.835					3.2	3.8	0.260
f_6	13.6605	158.107	0.62	4.7	0.11	7.9			1.313
f_{15}	13.9725	161.718			0.05	3.9			0.792
f_{17}	14.0608	162.740					5.2	6.2	0.471
f_{11}	15.0390	174.061			0.04	3.0	9.2	10.8	0.836
f_8	15.1787	175.678	6.46	6.1	0.18	13.7	12.1	14.0	0.979
f_{14}	15.8217	183.120	0.45	4.3	0.07	5.3			0.707
f_{13}	15.8344	183.267			0.14	9.7			0.726
f_4	16.0024	185.212	0.55	5.2	0.20	13.5			1.593
f_3	16.2507	188.086	1.04	9.6	0.16	10.9			1.736
f_1	17.1617	198.630	5.01	43.9	1.23	69.1	5.2	6.9	12.961
f_{12}	17.1863	198.914			0.12	6.7			0.692
f_9	17.2805	200.005			0.11	6.3	6.0	8.0	0.903

Notes. All were associated to a photometric term.

complex because of binarity, their average value was subtracted from the individual LSD profiles and the identification was performed on these residuals. A first identification was performed individually on each detected mode by fitting its amplitude and phase variations across the line profile. This supplied preliminary ℓ, m, i values. After that we performed a simultaneous fit of all modes with the previously detected ℓ, m values kept fixed, but leaving the inclination as free parameter. From the values of the discriminant we were able to estimate $i = 21° \pm 6°$ as the most probable inclination of the rotational axis (Fig. 15). Finally, a separate fit was performed on each detected mode assuming this inclination value to improve the ℓ, m values. The derived ℓ, m values are listed in Table 3, where the negative m values indicate retrograde modes. Uncertainties are estimated to be ±1 for the ℓ degree, while they are larger for the m values. The main cause for uncertainties are the contaminations by adjacent unresolved modes and by aliases. But the distinction between prograde and retrograde modes through the shape of the phase curves is quite unambiguous (see Fig. 13) and the total amplitude of these curves across the line profile supplies a good constraint to the ℓ value (Telting & Schrijvers 1997).

Knowing the inclination, we were able to estimate $v_{\rm eq} = 116 \pm 38$ km s^{-1} from the $v \sin i$ value and consequently the rotational frequency, $\nu_{\rm rot} = 0.67 \pm 0.32$ d^{-1}. We applied the same approach to the secondary component and estimated that it could be an F2 III star, with a bolometric absolute magnitude of 1.8 ± 0.3 mag, located just outside the red border of the instability strip.

3.6. Multicolour photometry

We also observed HD 50870 in Strömgren *uvby* photometry to have an independent tool to propose at least an identification of the modes with the highest amplitudes. *uvby* photometry was performed at San Pedro Mártir Observatory from 2007 to 2010 and the final dataset consists of 593 datapoints collected on 28 nights for a total survey of 156.5 h. The error on a single measurement is 0.005 mag in the *vby* filters and around 0.015 mag in *u* filter. The frequency analysis of this dataset allowed us to detect the terms from f_1 to f_5 in an unambiguous way. The aliasing effect is noticeable after the sixth term, since instead of $f_6 = 13.66$ d^{-1} the highest peak is the alias at f_6+1 d^{-1}. The subsequent residual spectrum became very noisy and the highest peaks cannot be identified in a reliable way with the frequencies detected in the CoRoT timeseries. Looking at the photometric amplitudes listed in Table 3, we infer that we were able to detect from ground all terms with a CoRoT amplitude higher than 1.0 mmag.

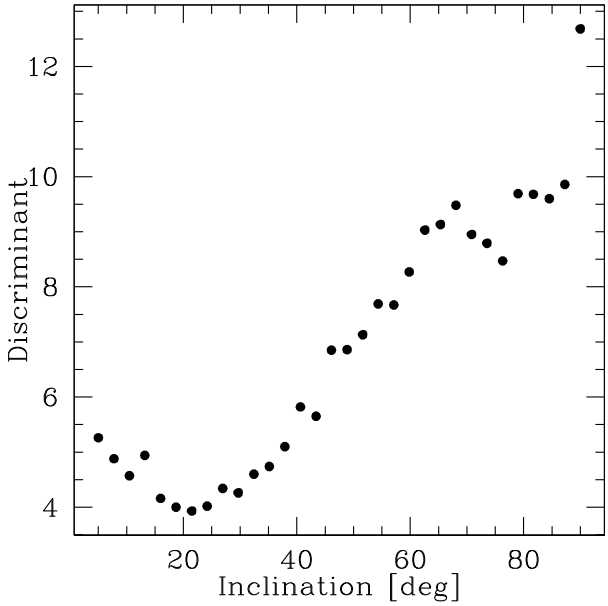

Fig. 15. Behaviour of the discriminant obtained by fitting all 19 spectroscopic modes simultaneously to the LSD profiles.

We calculated the amplitude ratios and phase shifts by using the *y* colour as reference system (Garrido 2000; Poretti et al. 2009). The predominant term f_1 is characterized by negative phase shifts (e.g., $\phi_v - \phi_y = -0.05 \pm 0.03$ rad, $\phi_b - \phi_y =$

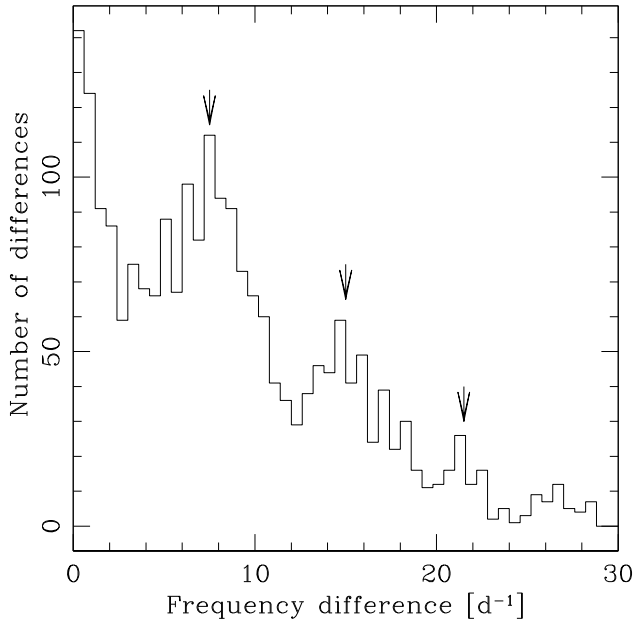

Fig. 16. Histogram of the differences between couples of frequencies with amplitudes higher than 0.1 mmag in the 0−30 d^{-1} interval. The pattern at 7.5, 15, and 22 d^{-1} is indicated.

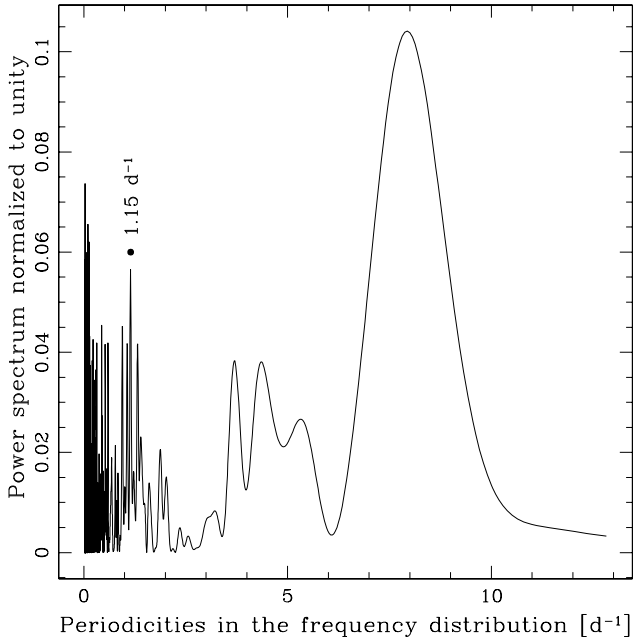

Fig. 17. Power spectrum derived from the distribution of the frequencies with amplitudes higher than 0.1 mmag. The strongest peak is close to the first peak of the pattern shown in Fig. 16. The peak at 1.15 d^{-1}, close to twice the rotational frequency, is also indicated.

-0.04 ± 0.03 rad). The amplitude ratios are $A_v/A_y = 1.39 \pm 0.04$ and $A_b/A_y = 1.19 \pm 0.05$. Therefore, the case of HD 50870 is different from that of HD 50844, where the positive phase shifts supported the identification of f_1 as radial mode (see Fig. 10 in Poretti et al. 2009). Here, the negative phase shifts suggest a nonradial mode, but this identification is ambiguous since the f_1 mode might belong to a high radial order (we obtain $Q = 0.014$ d from the procedure described in Sect. 3.5) and the theoretical phase shifts are negative in this case, too (see Fig. 13 in Garrido 2000). The phase shifts of the terms from f_2 to f_6 also have negative values, but the error bars are at least three times larger than that the f_1 ones, which precludes a reliable mode identification.

4. Frequency spacings

The asymptotic regime of the solar-like oscillations describes the well-known periodic pattern characterized by the large

$$\Delta\nu = \nu_{n+1,\ell} - \nu_{n,l} \quad (1)$$

and the small

$$\delta\nu = \nu_{n,\ell} - \nu_{n-1,\ell+2}. \quad (2)$$

separations. This regime is not valid for δ Sct stars and we were unable to detect the two separations as sharp structures in the frequency distributions; instead they appeared as quasi-regular spacings (García Hernández et al. 2009). These spacings become more evident when the search is restricted to the modes covering a small ℓ range. Because the modes with $\ell < 5$ should show the highest amplitudes, we performed our analysis by considering the frequencies with amplitudes higher than 0.1 mmag.

Searching for the large spacing (Fig. 16) we found a prominent peak around 7.5 d^{-1} and other peaks at 15 d^{-1} and 22 d^{-1}, i.e., about double and triple frequency of the former value. This suggests a regular pattern with a frequency separation of 7.5 d^{-1}. We also computed the Fourier power spectrum of a series of Dirac's δ functions with the same amplitude and centred on the frequencies detected in the CoRoT data. This power spectrum is characterized by a broad peak centred at about 7.8 d^{-1} (Fig. 17).

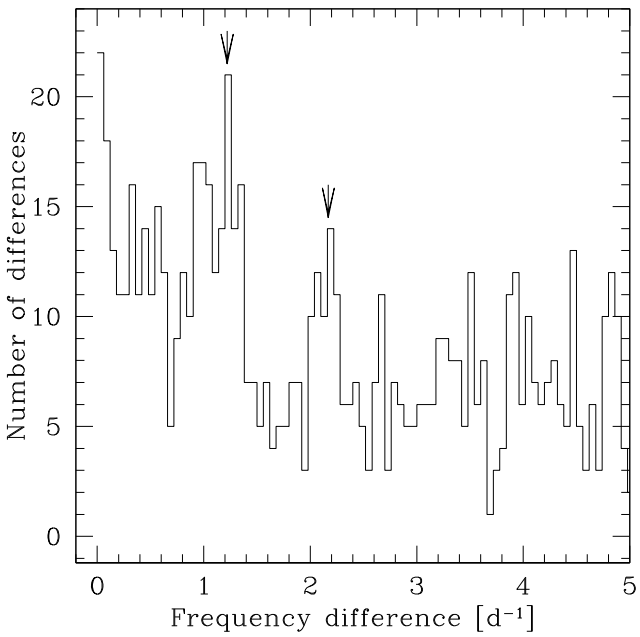

Fig. 18. Histogram of the differences between couples of frequencies with amplitudes higher than 0.1 mmag in the 0-5 d^{-1} interval. The peak at 1.2 d^{-1} and its double are visible.

When searching for a smaller regular spacing in the 0–5 d^{-1} interval, we were able to identify a prominent peak at about 1.2 d^{-1} (Fig. 18). The 1.2 d^{-1} value is approximately twice the rotational frequency (0.67 d^{-1}) and corresponds to the peak shown in Fig. 17. The recurrency of the 0.6 d^{-1} separation is confirmed by some peaks reproducing a multiplet pattern, as those observed at 6.70, 7.13, 7.66, 8.14, and 8.76 d^{-1}.

The study of the frequency spacings provided two main results. First, the Fourier transform and the histogram in the 0–5 d^{-1} range (Figs. 17 and 18) show the double of the rotational splitting, which is predicted for a frequency range high enough to render the effect of the Coriolis force negligible (Lignières et al. 2010). Second, the frequency differences in the 5–30 d^{-1} range show a spacing periodicity (as defined by García Hernández et al. 2009) of about 7.5 d^{-1}.

5. Asteroseismic modelling

The availability of the physical parameters and of the full description of the pulsational spectrum allowed us to perform the computation of asteroseismic models (i.e., equilibrium plus pulsation models), the analysis of instability, and a study of quasi-periodicities in the observed oscillation spectrum (García Hernández et al. 2009).

5.1. The asteroseismic models

Equilibrium models were computed with the evolutionary code CESAM (Morel 1997; Morel & Lebreton 2008). Physics included in the models was appropriate to the description of δ Sct stars (Casas et al. 2006). We considered a variation in the convective efficiency parameter $\alpha_{\rm MLT}$ up to 1.5, of the overshoot up to 0.3, and a solar metallicity. Diffusion and radiative forces were assumed to be negligible for this type of stars (Goupil et al. 2005) and were not included in the modelling. We considered about 2000 points for the computation mesh, following the studies of the Evolution and Asteroseismic Tools Activities (ESTA/CoRoT[1]; Moya et al. 2008; Lebreton et al. 2008).

We considered $i = 21° \pm 6°$ and then $v_{\rm eq} = 116 \pm 38$ km s^{-1}, as resulting from the spectroscopic mode identification. For these rotational velocities it is expected to find a non-rigid rotation in the stellar interior, in particular at the interface between the convective core and the radiative envelope. In that region the mixed modes (low-order p and g modes) have a significant sensitivity to variations of the internal rotation profile (Suárez et al. 2009). Without a detailed description of the shape of the internal rotation profile, we can reasonably approximate it with the physical assumption of a local conservation of the angular momentum during the evolution (Suárez et al. 2006) in the radiative zones, and a quasi-instantaneous transport of the angular momentum in the convective zones. The total angular momentum is conserved (no mass loss is expected during the main-sequence stage).

Pulsational models were obtained by a perturbation of the equilibrium models using the adiabatic oscillation code FILOU (Suárez 2002, and references therein). Models were computed using the physical parameters obtained from HARPS spectroscopy (see Table 2). The uncertainties in those parameters defined our space of validity for the representative models. Models were constrained to predict the highest amplitude modes having the expected spherical degrees (Table 3). This procedure defined two sets of models with masses of $M = 2.10$ and $2.18\,M_\odot$.

5.2. The instability analysis

A non-adiabatic analysis of the mode energy balance of the sets of models was performed with the GraCo code (Moya et al. 2004; Moya & Garrido 2008). Theoretical results were compared with the range covered by the spectroscopic modes and by most of the highest amplitude photometric modes, i.e., [6.5,18.4] d^{-1} (Tables 1 and 3). Each theoretical model is represented by a point in Fig. 19. We found a few models that predicted the over-stable region [6.5,18.4] d^{-1}. The analysis of instability thus constrains the representative models to a first set of models with $M = 2.18\,M_\odot$, $3.8692 < \log T_{\rm eff} < 3.8811$, $3.7003 < \log g < 3.7746$, $1.5009 < L/L_\odot < 1.5056$ and a second set with $M = 2.10\,M_\odot$, $3.8673 < \log T_{\rm eff} < 3.8803$, $3.7935 < \log g < 3.8529$, $1.3812 < L/L_\odot < 1.3886$.

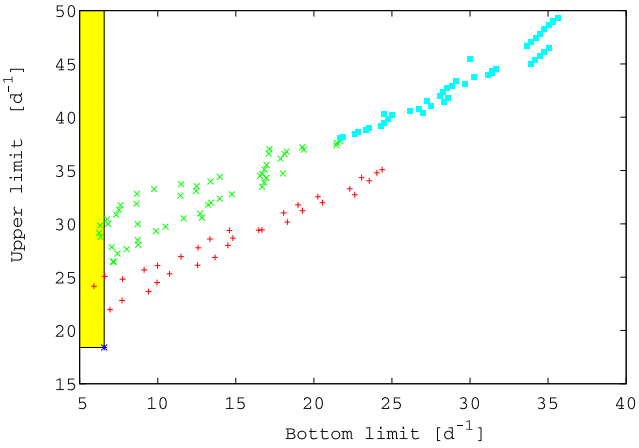

Fig. 19. Bottom versus upper limit of the instability range. Models computed using the physical parameters from spectroscopy are plotted as red and green crosses. The limits of the frequencies with the highest amplitudes observed in HD 50870 are depicted with a blue star. The shaded yellow area shows where a theoretical model must be to predict an over-stable frequency range containing the observed one. The models with a $\Delta\nu$ in the observed range of [3.5,4.5] d^{-1} are marked as light blue squares.

5.3. Analysis of quasi-periodic patterns

Using the aforementioned sets of theoretical models, we looked for quasi-periodic patterns. There is no model with a mean $\Delta\nu$ around 7.8 d^{-1} (Fig. 17). The pulsational models taking into account the rotational effects up to the second order of the perturbative approach did not point out structures similar to the multiplet centred at 7.66 d^{-1} (Sect. 4). Consequently, we considered the half value of 3.9 d^{-1}. We estimated the uncertainty of this value using the FWHM of the highest peak of the Fourier transform (Fig. 17). Thus, we obtained a [3.5,4.5] d^{-1} range for $\Delta\nu$. Models with $2.10\,M_\odot$ show these values, but they also predict a lower limit for the excited modes that is much higher than the observed one (Fig. 19).

Therefore, there is no model that at the same time predicts the [6.5,18.4] d^{-1} range of observed frequencies and the [3.5,4.5] d^{-1} range of the quasi-periodicity intepreted as a large separation. This seems a general problem in the era of rich pulsational spectra detected by space observations, as stressed by Uytterhoeven et al. (2011) when analysing the δ Sct stars observed with *Kepler*.

6. Discussion and conclusions

The space-based photometric and the ground-based spectroscopic monitorings of another δ Sct star after HD 50844 (Poretti et al. 2009) confirm that these variables show a complicated amplitude spectrum. HD 50870 has one predominant pulsation mode (17.1617 d^{-1}, 12.96 mmag), and about 20 modes

[1] http://www.astro.up.pt/corot/

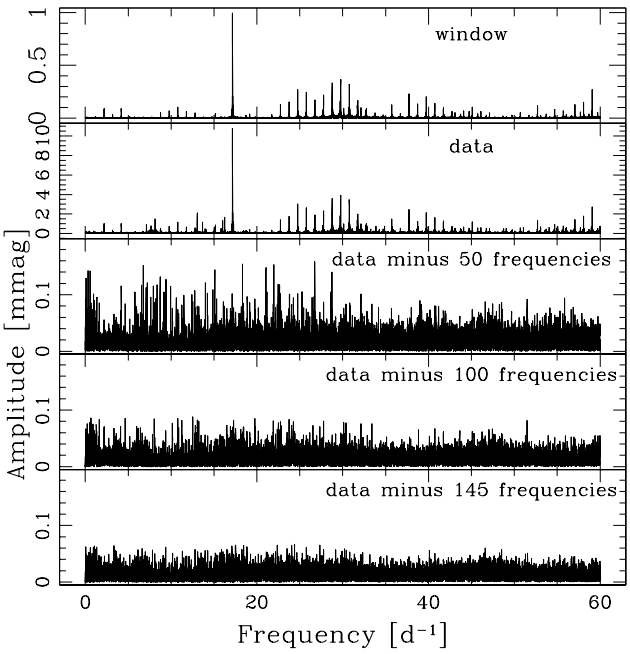

Fig. 20. Frequency analysis of the HD 50870 light curve but sampled with the data binning of the *Kepler* satellite. Only 145 peaks are detectable above the S/N level of 4.0. The spectral window shifted at the frequency of the predominant mode (17.16 d^{-1}) is shown in the *top panel*.

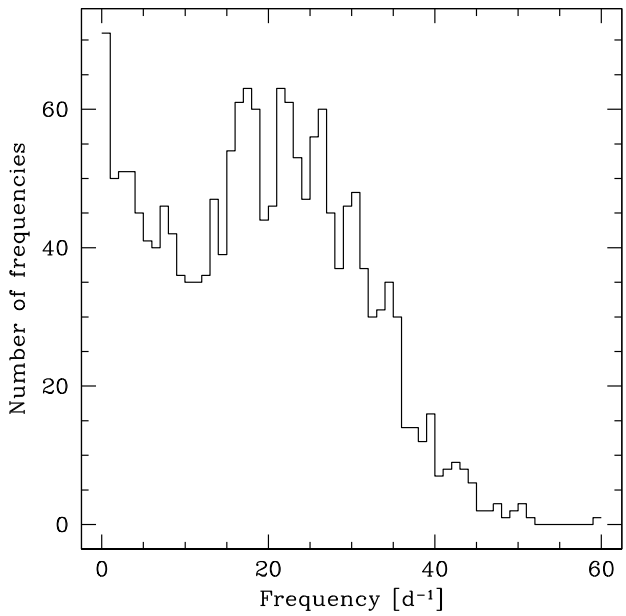

Fig. 21. Density distribution of the 1800 frequencies necessary to whiten the power spectrum (number of frequencies per d^{-1}) as a function of frequency.

with amplitudes beween 2.3 and 0.3 mmag and frequencies between 7 and 19 d^{-1}. Well-isolated peaks were detected down to 0.05 mmag. The frequencies with amplitudes lower than about 50 μmag ($S/N \sim 12$) form a flat low-frequency plateau with a cut-off at about 35d^{-1} (~400 μHz). After the detection of several hundreds of frequencies (down to amplitudes of about 12 ppm), there is still an excess of power at low frequencies (see last panel of Fig. 4). About 1800 frequency terms are necessary to obtain a flat power spectrum by means of a classical Fourier solution of the light curve.

The results obtained for HD 50870 confirm that we need hundreds of frequencies to reproduce the light curves of δ Sct stars, i.e., that HD 50844 is not an exception or a unique case (Balona & Dziembowski 2011). Because the light curves of δ Sct stars show rapid variations, the detailed investigation of the signal content must be performed on the basis of time series with a short cadence sampling. To illustrate the point, we grouped the CoRoT measurements of HD 50870 in bins of 30 min, i.e., the typical long cadence of the *Kepler* data. The resulting amplitude spectrum obtained from the frequency analysis of the 5135 datapoints is shown in Fig. 20. The spectrum is generally flat and a limited set of frequencies (145) is above the significance limit of 4.0. This can be explained by the fact that the pseudo-Nyquist frequency of the almost equally-spaced *Kepler*-like data is about 23 d^{-1}. Consequently, a consistent fraction of the spectral power below this limit (where most of the stellar signal is concentrated) is reflected above it, thus simulating a higher noise level. Indeed, we calculated a white noise level of 15 μmag (to be compared to the 3 μmag level obtained from the analysis with the CoRoT data sampling). We can conclude that the cadence of 30 min is unable to describe the light variation of δ Sct stars in a complete way.

We remain with the still unsolved problem whether the excess of power detected in the CoRoT timeseries below 50 d^{-1} is due to the excitation of a huge number of modes or is the result of a broad-band low-frequency noise process, i.e., we are observing a discrete or continuum power spectrum. A similar plateau has been observed by Poretti et al. (2009) in HD 50844 and it seems to be present in HD 174936, too (García Hernández et al. 2009). The analysis of the light variations of other δ Sct stars observed by CoRoT seems to support this result: HD 170699, for instance, which is a very fast rotator ($v \sin i = 270$ km s^{-1}) has a plateau with the cut-off at about 25 d^{-1} (Mantegazza et al., in prep.). A tentative preliminary answer can be given for HD 50870. The histogram that shows the distribution with a binning of 1 d^{-1} of the frequency terms needed to whiten the power spectrum (i.e., to lower its mean value at the low frequencies at about the same level as above 60 d^{-1}) is shown in Fig. 21. Excluding the peak close to zero frequency, which might be affected by the residual satellite low-frequency noise, the maximum density is 63 frequencies per d^{-1}, with an average value below ~35 d^{-1} of about 50 frequencies per d^{-1}. It is well known that if we have a time series generated by a process with a continuum power spectrum, and we estimate its power spectrum by means of the discrete Fourier transform, we approximate it with a discrete spectrum consisting of a bunch of peaks with a separation between them of the order of the reciprocal of the time series baseline (e.g., Chatfield 1984). The baseline of the CoRoT observations is about 114 d, therefore we should expect a frequency density of the order of 114 frequencies per d^{-1} to be detected if there is a signal with a continuum power spectrum. Since the observed density is decidedly lower, this analysis rules out the possibility that the plateau is due to a process with a continuum power spectrum. However, it does not rule out the action of the granulation effect, since this effect could be described as a random process with characteristic time scales that could generate different densities. The observed frequency ranges, amplitudes, and densities pose observational constraints to the models of the convective layers in δ Sct stars, at the moment limited to temperatures cooler than that of HD 50870 ($T_{\rm eff} < 6850$ K, Samadi et al. 2002). A more detailed theoretical investigation is necessary to support the effectiveness of convection in δ Sct stars.

As for HD 50844, high-resolution spectroscopy was of paramount importance to improve the physical scenario. The

analysis of the line profile variations allowed us to identify nineteen progrades, axisymmetric and retrogrades modes having $\ell \leq 9$ as well as an inclination angle of about 21°. The corresponding rotational velocity is about 116 km s^{-1}, and therefore HD 50870 is rotating at about 34% of the break-up velocity.

HARPS spectroscopy suggests that the predominant mode is axisymmetric ($m = 0$), but it does not allow us to distinguish between a radial or a nonradial mode. The greater difference between a radial mode ($\ell = 0$) and an axisymmetric nonradial one with $\ell = 1$ is in the equatorial region, but in the current case of a star seen almost pole-on this region supplies a very limited contribution through the Doppler effect to the overall line profile variations. On the other hand, the Baade-Wesselink technique (Sect. 3.5) and the amplitude ratios and phase shifts in different photometric colours (Sect. 3.6) seem to indicate a nonradial mode. More in general, despite the huge observational effort, there is still a mismatch between the observational contraints and the theoretical modelling. The mechanism of selecting the modes with the highest amplitudes is not yet fully understood, also when considering the effect of fast or moderate rotation.

Antoci et al. (2011) observed a 0.1−0.2 mmag level of the solar-like oscillations for HD 187547. We did not find any evidence of the presence of oscillations like this in HD 50870, at least above the level of 12 ppm. The non-detection may be the result of the dilution of the structures broadened by the mode lifetime into the noise and an apparent reduced amplitude due to the light from the companion. In both cases, the damping should be very effective to produce a null detection. HD 187547 has physical parameters very similar to those of HD 50870, but also a slight overabundance of some chemical elements. Since the amplitude of solar-like oscillations depends on the surface metal abundance (Samadi et al. 2010a,b), this particularity can explain why the visibility of these oscillations is enhanced in HD 187547. A well-hidden cooler companion could also be an explanation for the case of HD 187547 because we were able to detect the binarity of HD 50870 only thanks to the continuous monitoring with high-S/N HARPS spectra.

Acknowledgements. The HARPS data are being obtained as part of the ESO Large Programmes LP 182.D-0356 and LP 185.D-0056 (PI.: E. Poretti). Mode identification results were obtained with the software package FAMIAS developed in the framework of the FP6 Coordination Action Helio- and Asteroseismology (HELAS; http://www.helas-eu.org/). E.P. thanks J. Ballot, F. Lignières, and M. Pasek for enlightning discussions during his stay at IRAP, Toulouse. We thank J. Vialle for checking the English form of the original manuscript. P.J.A. acknowledges financial support from grants AYA2009-08481-E and AYA2010-14840 of the Spanish Ministry of Science and Innovation (MICINN). A.M. acknowledges the funding of AstroMadrid (CAM S2009/ESP-1496) and the Spanish grants ESP2007-65475-C02-02, AYA 2010-21161-C02-02. J.C.S. acknowledges the financial support from the Spanish Ministry of Science through its *Plan Nacional del Espacio* under project AYA2010-12030-E and AYA2010-20982-C02-01. This work was supported by the Italian PRIN-INAF 2010 *Asterosesismology: looking inside the stars with space- and ground-based observations*.

References

Antoci, V., Handler, G., Campante, T. L., et al. 2011, Nature, 477, 570
Auvergne, M., Bodin, P., Boisnard, L., et al. 2009, A&A, 506, 411
Baglin, A., Auvergne, M., Barge, P., et al. 2006, ESA SP, 1306, 33
Balona, L. A., & Dziembowski, W. A. 2011, MNRAS, 417, 591
Breger, M. 2000, in Delta Scuti and Related Stars, ed. M. Breger, & M. H. Montgomery, ASP Conf. Ser., 210, 3
Breger, M., Lenz, P., Antoci, V., et al. 2005, A&A, 435, 955
Casas, R., Suárez, J. C., Moya, A., & Garrido, R. 2006, A&A, 455, 1019
Chatfield, C. 1984, The analysis of Time Series: An Introduction (London-New York: Chapman and Hall)
Daszynska-Daszkiewicz, J., Dziembowski, W. A., & Pamyatnykh, A. A. 2006, Mem. Soc. Astron. Ital., 77, 113
Deeming, T. J. 1975, Ap&SS, 36, 137
Donati, J.-F., Semel, M., Carter, B. D., Rees, D. E., & Collier Cameron, A. 1997, MNRAS, 291, 658
Garrido, R. 2000, in Delta Scuti and Related Stars, ed. M. Breger, & M. H. Montgomery, ASP Conf. Ser., 210, 67
García Hernández, A., Moya, A., Michel, E., et al. 2009, A&A, 506, 79
Goupil, M.-J., Dupret, M. A., Samadi, R., et al. 2005, J. Astrophys. Astron, 26, 249
Ilijic, S. 2004, ASP Conf. Ser., 318, 107
Ilijic, S., Hensberge, H., Pavloski, K., & Freyhammer, L. M. 2004, ASP Conf. Ser., 318, 111
Kallinger, T., & Matthews, J. M. 2010, ApJ, 711, L35
Kupka, F. G., Ryabchikova, T. A., Piskunov, N. E., et al. 2000, Baltic Astron., 9, 590
Lebreton, Y., Monteiro, M. J. P. F. G., Montalbán, J., et al. 2008, Ap&SS, 316, 1
Lenz, P., & Breger, M. 2005, CoAst, 146, 53
Lignières, F., & Georgeot, B. 2009, A&A, 500, 1173
Lignières, F., Georgeot, B., & Ballot, J. 2010, AN, 331, 1053
Mantegazza, L. 2000, in Delta Scuti and Related Stars, ed. M. Breger, & M. H. Montgomery, ASP Conf. Ser., 210, 138
McCuskey, S. W. 1956, ApJS, 2, 271
Moya, A., & Garrido, R. 2008, Ap&SS, 316, 129
Moya, A., Garrido, R., & Dupret, M. A. 2004, A&A, 414, 1081
Moya, A., Christensen-Dalsgaard, J., Charpinet, S., et al. 2008, Ap&SS, 316, 231
Morel, P. 1997, A&AS, 124, 597
Morel, P., & Lebreton, Y. 2008, Ap&SS, 316, 61
Piskunov, N. E., Kupka, F., Ryabchikova, T. A., et al. 1995, A&AS, 112, 525
Poretti, E., Alonso, R., Amado, P. J., et al. 2005, ApJ, 129, 2461
Poretti, E., Michel, E., Garrido, R., et al. 2009, A&A, 506, 85
Rainer, M. 2003, Laurea Thesis (in Italian), Università degli Studi di Milano
Reegen, P. 2007, A&A, 467, 1353
Samadi, R., Goupil, M.-J., & Houdek, G. 2002, A&A, 395, 563
Samadi, R., Ludwig, H.-G., Belkacem, K., Goupil, M.-J., & Dupret, M.-A. 2010a, A&A, 509, A15
Samadi, R., Ludwig, H.-G., Belkacem, K., et al. 2010b, A&A, 509, A16
Schaller, G., Schaerer, D., Meynet, G., & Maeder, A. 1992, A&AS, 96, 269
Stamford, P. A., & Watson, R. D. 1981, Ap&SS, 77, 131
Straiziys, V., & Kuriliene, G. 1981, Ap&SS, 80, 353
Stuetz, Ch., Bagnulo, S., Jehin, E., et al. 2006, A&A, 451, 285
Suárez, J. C. 2002, Ph.D. Thesis, ISBN 84-689-3851-3, ID 02/PA07/7178
Suárez, J. C., Goupil, M. J., & Morel, P. 2006, A&A, 449, 673
Suárez, J. C., Moya, A., Amado, P. J., et al. 2009, ApJ, 690, 1401
Telting, J. H., & Schrijvers, C. 1997, A&A, 317, 723
Uytterhoeven, K., Moya, A., Grigahcène, A., et al. 2011, A&A, 534, A125
Valenti, J. A., & Piskunov, N. 1996, A&A, 118, 595
Zima, W. 2008, CoAst, 155, 17